BMC Medical Imaging

RESEARCH

Open Access

Quantitative evaluation of pancreatic neuroendocrine tumors utilizing dual-source CT perfusion imaging

Ge Liu[1†], Yan-Jun Gao[1†], Xiao-Bing Li[2], Yi Huan[4], Jian Chen[2] and Yan-Meng Deng[3*]

Abstract

Objective We aimed to quantitatively analyze the perfusion characteristics of pancreatic neuroendocrine tumors (pNETs) utilizing dual-source CT imaging.

Methods Dual-source CT perfusion scans were obtained from patients with pNETs confirmed by surgical or biopsy pathology. Perfusion parameters, including blood flow (BF), blood volume (BV), capillary permeability surface (PS), mean transit time (MTT), contrast transit time to the start (TTS), and contrast transit time to the peak (TTP), were statistically analyzed and compared with nearby healthy tissue. Time density curves (TDCs) were plotted to further understand the dynamic enhancement characteristics of the tumors. Additionally, receiver operating characteristic curves (ROCs) were generated to assess their diagnostic value.

Results Twenty patients with pNETs, containing 26 lesions, were enrolled in the study, including 6 males with 8 lesions and 14 females with 18 lesions. The average values of BF, BV, PS, MTT, TTP and TTS for the 26 lesions (336.61 ± 216.72 mL/100mL/min, 41.96 ± 16.99 mL/100mL, 32.90 ± 11.91 mL/100 mL/min, 9.44 ± 4.40 s, 19.14 ± 5.6 s, 2.57 ± 1.6 s) were different from those of the adjacent normal pancreatic tissue (44.32 ± 55.35 mL/100mL/min, 28.64 ± 7.95 mL/100mL, 26.69 ± 14.88 mL/100 mL/min, 12.89 ± 3.69 s, 20.33 ± 5.18 s, 2.69 ± 1.71 s). However, there were no statistical differences in PS and TTS between the lesions and the adjacent normal pancreatic tissue ($P > 0.05$). The areas under the ROC curve for BF, BV, and PS were all greater than 0.5, whereas the areas under the ROC curve for MTT, TTP, and TTS were all less than 0.5.

Conclusion CT perfusion parameters such as BF, BV, MTT, and TTP can distinguish pNETs from healthy tissue. The area under the ROC curve for BF, BV, and PS demonstrates substantial differentiating power for diagnosing pNET lesions.

Keywords Differential diagnosis, Dual-source CT, Pancreatic neuroendocrine tumors, Radiology

[†]Ge Liu and Yan-Jun Gao contributed equally to this work.

*Correspondence:
Yan-Meng Deng
yanmengdengdym@126.com
[1]Department of Radiology, Xi'an No. 3 Hospital, the Affiliated Hospital of Northwest University, Xi'an, Shaanxi 710018, China
[2]Department of Peripheral Vascular Medicine, Xi'an Honghui Hospital, Xi'an, Shaanxi 710018, China
[3]Center of Radiology, Shaanxi Traditional Chinese Medicine Hospital, Xi'an, Shaanxi 710003, China
[4]Department of Radiology, The First Hospital of Air Force Medical University, Xi'an, Shaanxi 710032, China

Introduction

Pancreatic neuroendocrine tumors (pNETs) are rare, accounting for less than 3% of all primary pancreatic tumors [1, 2]. Advances in imaging and pathological immunohistochemistry have significantly enhanced our understanding of pNETs in recent years. According to the 2010 "Digestive System Tumors WHO Classification," all pNETs possess some degree of malignant potential [3, 4]. Notably, the incidence of liver metastases from pNETs is as high as 85% [5, 6]. Surgical resection remains the most effective treatment, underscoring the importance of accurately locating tumor tissue.

Imaging plays a critical role in determining the location of pNETs, evaluating tumor invasion into surrounding tissues, and detecting peripheral lymph nodes and liver metastasis [7–10]. Currently, CT, MRI, and ultrasound are the primary imaging modalities used for pancreatic evaluation. While ultrasound can serve as a screening tool, its accuracy in identifying abnormal tissue is limited. CT, with rapid scanning capabilities and high spatial-temporal resolution, offers highly sensitivity, specificity, and accuracy in detecting pancreatic lesions. As a result, CT has become the preferred imaging method for evaluating pancreatic masses. Many researchers have employed multi-phase dynamic CT scans to diagnose pNETs, finding that most functional pNETs exhibit a "fast in and fast out" enhancement pattern due to their rich vascularity.

However, some tumors are less vascular or even cystic, which can lead to misdiagnosis or missed detection. Recent studies have reported varying sensitivities of multi-phase dynamic enhanced CT in detecting pNETs, ranging from 54.3 to 75.1% [11–13]. This variability is attributed to the diverse enhancement patterns of pNETs, including persistent arterial-phase enhancement and transient early arterial phase hyperenhancement [14]. Furthermore, approximately 24.9% of pNET lesions appear iso-enhanced on multi-phase dynamic enhanced CT images, making accurate diagnosis challenging [13]. Therefore, traditional multiphase dynamic enhanced CT may not fully meet the diagnostic requirements of pNETs.

CT perfusion scanning involves dynamically imaging the target area following a bolus injection of contrast agent via the anterior cubital vein. In clinical practice, numerous researchers have employed CT perfusion imaging to assess pancreatic tumors, with some utilizing it for tumor localization and grading [15–17]. In the investigation of CT perfusion research concerning pancreatic-related conditions, the majority of studies have centered on normal pancreatic tissue, pancreatitis, and pancreatic cancer. Most pNETs are rich in blood supply. Therefore, the diagnostic rate of this lesion may be improved by analyzing various perfusion parameters of CT perfusion. There is a noticeable dearth of research on CT perfusion parameters specific to pNETs. The study aimed to quantitatively analyze the perfusion characteristics of pNETs utilizing dual-source CT imaging, so as to improve the diagnostic accuracy of pNETs, promote early clinical treatment, and potentially improve the survival rate of patients.

Materials and methods

Patients

Between October 2022 and December 2023, we prospectively enrolled a cohort of 20 patients confirmed to have pNETs through either surgical pathology or needle biopsy. Ethical approval for the study was obtained from the Ethics Committee of Xi'an No.3 Hospital. Inclusion criteria were as follows: (1) age ≥ 18 years old; (2) recurrent hypoglycemia or hyperglycemia; (3) pancreatic space revealed by abdominal ultrasound or CT scan. Patients with a history of hyperthyroidism, asthma, or iodine allergy were excluded.

Additionally, the diameter of the target lesion needed to be greater than 10 mm, and informed consent was obtained from the participants. Exclusion criteria included unconsciousness or an inability to cooperate, as well as concurrent heart or kidney insufficiency. Pregnant women were also excluded from participation.

Image acquisition and processing

Scanning method

We utilized a dual-source CT (Definition Flash, Siemens Healthcare, Forchheim/Germany) for all patient scans. Patients were instructed to fast for at least 4 h before the examination. Approximately 30 min before the scan, they were given a moderate amount of warm water to fill the stomach and duodenum. Patients were positioned supine and instructed to breathe shallowly to minimize movement artifacts, with an abdominal belt provided if needed for stabilization.

The scan protocol began with abdominal localization imaging, followed by a routine abdominal CT scan to define the range for perfusion scanning. A high-pressure syringe was used to inject 60 mL of non-ionic contrast agent (iopromide, Ultravist®, Bayer Schering Pharma) at a concentration of 370 mgI/mL through the elbow vein, followed by a 40 mL bolus injection of 0.9% sodium chloride solution at a rate of 5.0 mL/s. CT perfusion scanning was performed using the body VPCT Dynmulti 4D scanning mode (also known as the "cradle bed" mode). The scan parameters were as follows: tube voltage: 100 kV; tube current: 120 mA; matrix: 512×512; collimator

width: 32×1.2 mm; rotation time: 0.28 s; convolution kernel: B20; scanning layer thickness: 1.2 mm; reconstruction layer thickness: 3 mm; delay: 6 s; total collected points: 22; interval time: 2s; total time: 45.32 s.

Image post-processing

Perfusion scan data were transferred to a Siemens Syngo Multi-Modality workstation (MMWP, Siemens Healthcare, Forchheim, Germany) for analysis. The VPCT Body (Somaris/s syngo CT 2013 A) software was used to load the perfusion images, apply motion correction, and perform 4D noise reduction. The threshold range was set between −50 and 250 HU, with the abdominal aorta serving as the input artery. The deconvolution model was used to calculate the region of interest (ROI) and generate the perfusion pseudo-color map along with perfusion parameters of adjacent normal pancreatic tissue. These parameters included blood flow (BF), blood volume (BV), capillary surface permeability (PS), mean transit time (MTT), contrast transit time to the start (TTS), and contrast transit time to the peak (TTP).

Selection of ROI

Given the typically small size of pNETs, the largest and most solid component of the tumor was selected for measuring perfusion parameters. Adjacent normal pancreatic tissue was also analyzed for comparison. Each measurement was performed three times, and the average of the values was used to ensure accuracy. During ROI selection, care was taken to exclude areas such as the pancreatic duct, blood vessels, tumor margin, and any necrotic or calcified regions within the tumor capsule.

Image analysis

Two experienced radiologists, blinded to the pathological results, independently analyzed the CT perfusion images of all 20 patients. In cases of disagreement, a consensus was reached through consultation between the two radiologists.

Statistical analysis

The measurement data were presented as mean ± SD, and a paired t-test in SPSS 17.0 software was utilized to compare the perfusion parameters of pNET lesions and the surrounding normal pancreatic tissue. Statistical significance was set at $p<0.05$. The diagnostic performance was assessed by area under the curve (AUC) based on ROC curves for perfusion parameters generated using SPSS 17.0. The cutoff values were determined using Youden index with sensitivity and specificity.

Results

General clinicopathological data

This study included 20 patients diagnosed with pNETs, with a total of 26 lesions identified. Among them, six males had eight lesions, and 14 females had 18 lesions. The patients' ages ranged from 24 to 79 years, with an average age of 49.1 ± 14.5 years. Of the 26 lesions, 23 were confirmed through surgical pathology. Additionally, five patients were also diagnosed with type I multiple endocrine neoplasia (MEN1): one patient had three small insulinomas, one pituitary microadenoma, and a left adrenal adenoma; another patient had one small insulinoma and a left adrenal adenoma; two patients had two gastrinomas each, and one patient had two non-functional pNETs.

Four lesions were situated in the pancreatic head, three in the uncinate process, four in the pancreatic neck, nine in the pancreatic body, five in the pancreatic tail, and one in both the body and tail of the pancreas. The tumor diameters ranged from 1.0 to 7.0 cm, with an average size of 1.95 ± 1.64 cm. Among these tumors, 19 were functional pNETs, including 15 insulinomas, two gastrinomas, one glucagonoma, and one mixed tumor consisting of an insulinoma and vasoactive intestinal peptide tumor. The clinical presentations of functional pNETs mainly manifested as hypoglycemia, accompanied by intermittent symptoms such as dizziness, fatigue, unconsciousness, diarrhea, diabetes, and peptic ulcers. Additionally, seven non-functional pNETs were identified. Four of these were incidentally discovered during routine physical examinations without any associated clinical symptoms, while the remaining three were detected due to abdominal discomfort, abdominal pain, weight loss, and low back pain. Among the 26 lesions, 23 were categorized as highly differentiated pNETs, including 19 G1 lesions, four G2 lesions, and three poorly differentiated lesions categorized as pancreatic neuroendocrine carcinomas (G3).

Imaging features of CT perfusion

Based on the CT perfusion images, the enhancement patterns of the 26 lesions were categorized into three distinct types (Figs. 1, 2 and 3). Among them, 15 lesions exhibited a "fast-in and fast-out" pattern (Fig. 4), characterized by significant enhancement during the early arterial phase followed by a rapid reduction or equivalent enhancement to the pancreas during the portal phase (with equivalence noted in the delayed phase). Eight lesions displayed a "fast in and slow out" pattern (Fig. 5), showing substantial enhancement during the arterial phase, with subsequent enhancement higher than the pancreas during the portal phase, and slightly higher than the pancreas in the delayed phase. Lastly, three lesions demonstrated a "slow in and slow out" pattern (Fig. 6), featuring slight

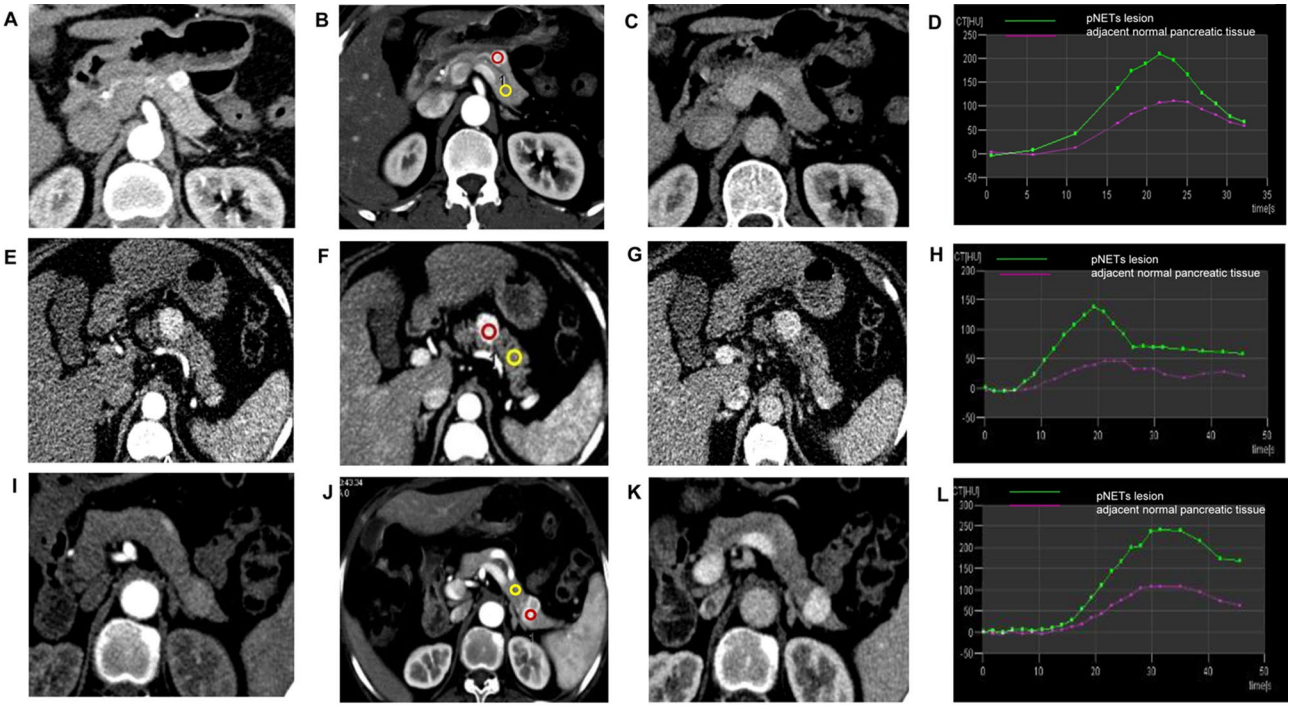

Fig. 1 The enhancement of G1 grade functional pNETs in different parts of the pancreas. (**A**-**D**): pNETs in the pancreatic body. (**E**-**H**): pNETs in the pancreatic neck. (**I**-**L**): pNETs in the pancreatic tail. (**A**-**C**), (**E**-**G**) and (**I**-**K**) are the perfusion images of the lesion in the arterial, portal and delay phase, respectively. The red and yellow circles in (**B**), (**F**) and (**G**) show the selection of the region of interest of the pNET lesion and adjacent normal pancreatic tissue. **D**, **H**, and **L** are time density curves of the lesion

to moderate enhancement during the arterial phase, slightly higher than the pancreas in the portal phase, and either equal to or slightly higher than the pancreas in the delayed phase.

Factors analysis

The mean values of BF, BV, MTT, and TTP differed between the 26 pNET lesions and adjacent normal pancreatic tissues ($P<0.05$), whereas no statistical difference was observed in PS and TTS between the two groups ($P>0.05$) (Table 1). Among the 23 well-differentiated pNETs (G1/G2) and adjacent normal pancreatic tissues, all perfusion parameters showed statistically significant differences ($P<0.01$), except for TTS (Table 2). The mean values of BF, BV, PS, and MTT for the three poorly differentiated pNETs (G3) were 75.16±43.21 mL/100 mL/min, 8.51±2.54 mL/100 mL, 24.77±10.11 mL/100 mL/min, and 8.97±1.27 s, respectively, which were all lower than those of the 23 well-differentiated pNETs. The TTP and TTS for the three poorly differentiated pNETs (G3) were 19.94±6.91 s and 1.75±0.83 s, respectively (Table 3). The AUC values for BF, BV, and PS were 0.883, 0.886, and 0.752, respectively, while the AUC values for MTT, TTP, and TTS were less than 0.5 (Fig. 7; Table 4).

Discussion

CT perfusion imaging generates a TDC that reflects the dynamic progression of contrast agent distribution within the organ over time, indirectly indicating organ blood perfusion. Parameters such as BF, BV, MTT, and PS of the contrast agent can be calculated from this data [18, 19]. These metrics help assess tissue and organ perfusion status and are widely applied in evaluating conditions affecting the brain, abdomen, and pelvis [20]. In oncology, perfusion imaging plays a crucial role in tumor detection, staging, and assessing vascular origin. For example, in pancreatic cancer, BF and BV are significantly lower compared to normal pancreatic tissue, while neuroendocrine tumors display increased perfusion, exhibiting distinct perfusion characteristics from pancreatic cancer [21].

Pancreatic perfusion imaging combines morphological and functional insights to enhance the diagnostic accuracy of pancreatic disorders [22]. In the diagnosis of pancreatic cancer, imaging during the pancreatic parenchymal phase is essential, as it optimally reveals the poor vascularity typical of pancreatic cancer, making lesions more conspicuous. In contrast, neuroendocrine tumors, which are highly vascularized, show early arterial phase enhancement. Hence, arterial phase imaging is ideal, and perfusion scanning proves to be an effective strategy for avoiding misdiagnoses [23]. Previous studies found

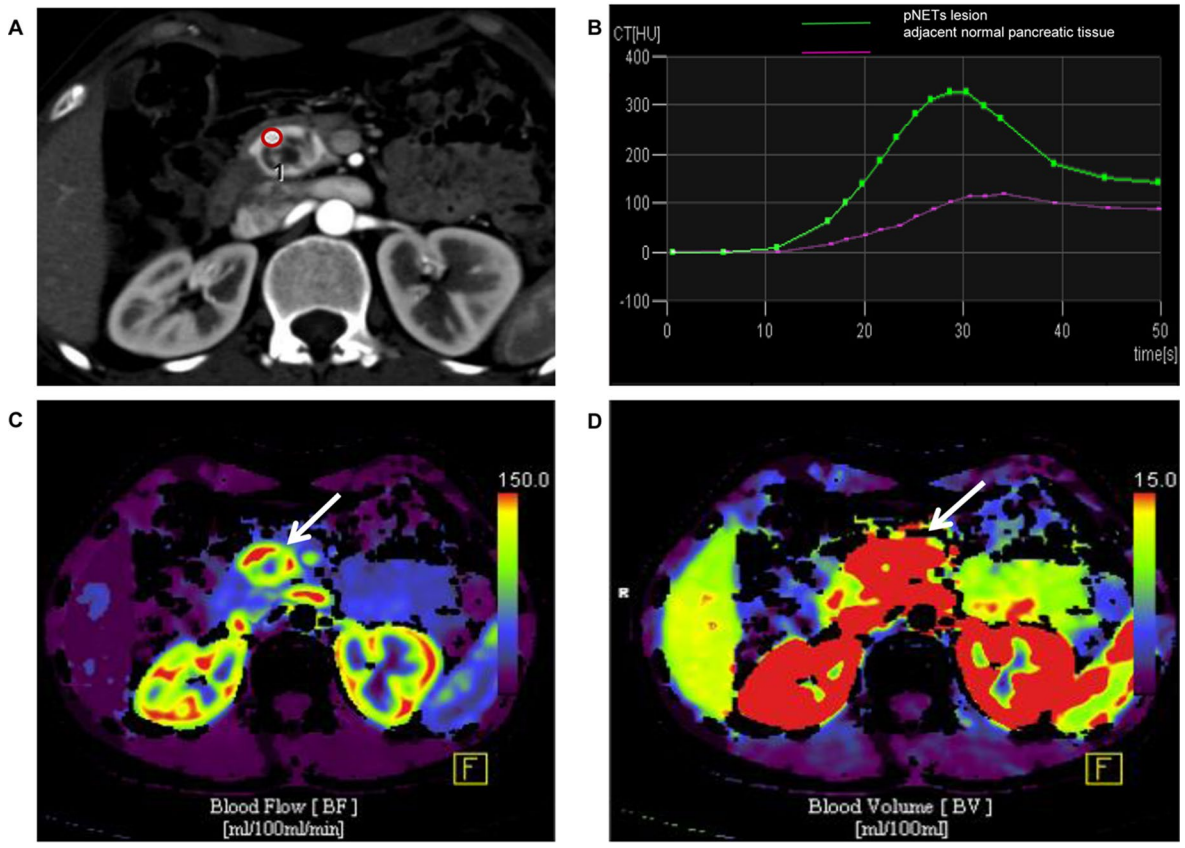

Fig. 2 G1 grade non-functional pNET in the head of the pancreas. (**A**) is the enhancement of the lesion in the arterial phase. (**B**) is the TDC curve, showing that the solid part of the lesion has a higher degree of enhancement than the surrounding normal pancreas. (**C**) and (**D**) are pseudo-color images of the BF and BV perfusion in the lesion area, respectively. The arrows show the high perfusion areas

that compared with conventional computer-enhanced scanning, CT perfusion imaging had a higher diagnostic accuracy in the diagnosis of neuroendocrine tumors, with a detection rate of 89.1% [23].

In this study, pancreatic perfusion scanning was conducted using dual-source CT. Compared to other multislice spiral CT perfusion techniques, dual-source CT scans offer several advantages. Firstly, they utilize two sets of x-ray tubes, a detector system, and a 128-slice sector, which enhance scanning speed, reduce scan duration, and diminish the impact of respiratory motion artifacts. Secondly, a large pitch and reciprocating "cradle bed" intermittently adopt the point scanning mode, effectively minimizing exposure time [24–26]. In our study, the exposure time was 2 s, and a total of 22 points were collected to minimize radiation dosage.

The current study involved statistical analysis and comparison of perfusion parameters between 26 pNET lesions and the surrounding normal pancreatic tissue. The findings revealed that the average values of BF, BV, and PS in pNETs were higher compared to those in the adjacent normal pancreatic tissue. However, the differences in BF and BV from normal pancreatic tissue were statistically significant, consistent with previous findings [27]. The findings might improve the diagnostic accuracy of pNETs, promote early clinical treatment, and potentially improve the survival rate of patients.

In addition, perfusion parameters including BF and BV, MTT, and TTP might help determine the scope of resection. However, further prospective study with a large sample of patients is needed. Conversely, although the PS value of pNETs showed some variation compared to normal pancreatic tissue, this difference was not statistically significant, contradicting previous reports [27]. The PS value is associated with various factors including tumor cells, fibrous hyperplasia, residual normal pancreatic tissue, and cystic necrotic tissue. Therefore, a lower PS value indicates a higher tumor malignancy.

In our study, only three cases of neuroendocrine carcinoma (G3) were identified among the 26 lesions analyzed. Comparison of the PS values between the 23 well-differentiated pNETs (G1/G2) and adjacent pancreatic tissues revealed significant differences, further supporting the notion that PS value correlates with tumor malignancy and can serve as an indicator for tumor grading. Moreover, both MTT and TTP values of pNETs were smaller

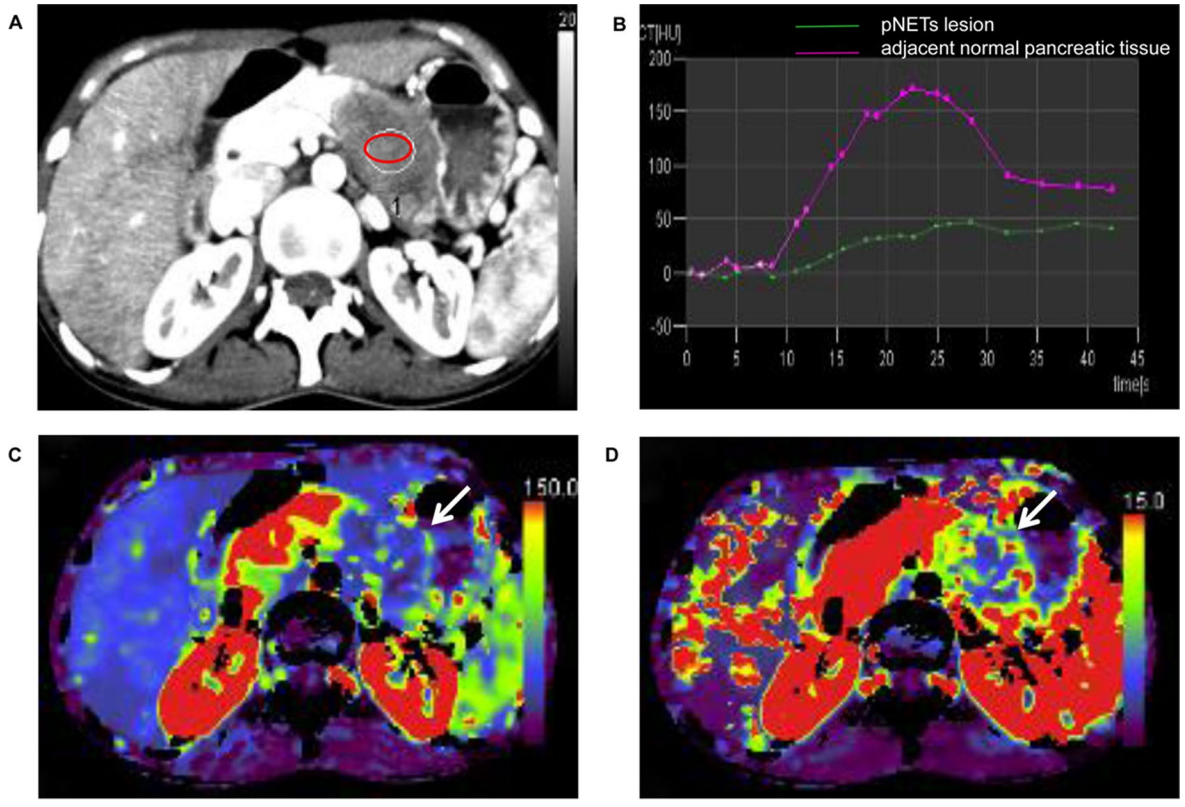

Fig. 3 G3 grade pNET in the tail of the pancreas. (**A**) is the enhancement performance in the arterial phase of the lesion. (**B**) is the TDC curve. (**C**) and (**D**) are pseudo-color images of the BF and BV perfusion in the lesion area, respectively. The arrows show that the tumor perfusion is low with a small amount of spot-like hyper-perfusion inside

compared to those of the surrounding normal pancreatic tissue, while TTS was similar to normal pancreatic tissue, consistent with previous findings [25]. The perfusion parameters of the three poorly differentiated pNETs were lower than those of the 23 well-differentiated pNETs and the normal pancreatic tissue. Hence, CT perfusion imaging is considered capable of predicting biological behavior and distinguishing and grading diseased tissue from benign and malignant tissue [28]. Literature reports indicate that the perfusion volume of tumors with high drug sensitivity may change between pre-and post-treatment conditions, suggesting that perfusion CT can also assess the therapeutic efficacy of tumors [29].

Furthermore, the area under the ROC curves for BF, BV, and PS were 0.883, 0.886, and 0.752, respectively, all exceeding 0.5, indicating significant diagnostic value. Conversely, the area under the ROC curves for MTT, TTP, and TTS were all below 0.5, suggesting no diagnostic utility. The cut-off values for BF, BV, and PS were determined to be 205.30 mL/100 mL/min, 30.52 mL/100 mL, and 25.1 mL/100 mL/min, respectively. Thus, when the values of BF, BV, and PS surpass these thresholds, the presence of pNETs should be considered. Upon plotting the ROC curves for BF, BV, and PS, slight convergence of the ordinate and abscissa lines was observed, likely due to differences in values within the group. Subsequently, data exhibiting large disparities between the tumor and surrounding normal tissues were excluded, resulting in more realistic ROC curves with increased area under the curve and sensitivity. This underscores the potential of BF, BV, and PS in tumor grading for diagnosing highly differentiated pNETs.

pNETs are heterogeneous tumors, of which rich blood supply is a typical imaging sign. The disease often needs to be differentiated from pancreatic rich blood supply lesions, such as pancreatic accessory spleen and pancreatic solid serous cystadenoma (sSCA). It is easy to distinguish the accessory spleen from functional PNETs by the presence or absence of clinical symptoms, but slightly difficult to distinguish from non-functional pNETs. The accessory spleen is generally located near the spleen, with uniform density and blood supply mainly coming from the splenic artery, and the enhancement degree of the enhanced scan is the same as that of the spleen, so it can be used as a differentiating point [30]. It is difficult to distinguish pNETs from sSCA, which are similar in morphological changes and indirect signs. Because sSCA has higher water content than other solid pancreatic tumors, it is characterized by low density on CT plain scan. Previous studies have found that the enhancement of blood

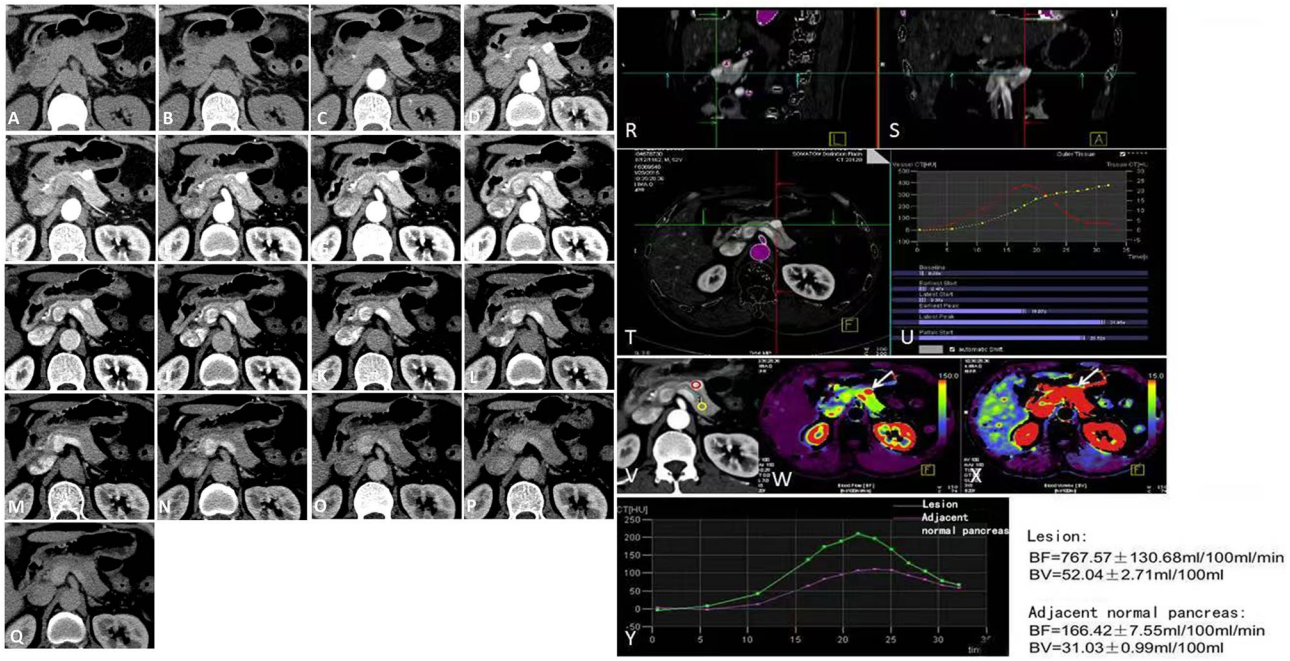

Fig. 4 Representative case with "fast-in and fast-out" enhancement of lesions. The male was 52 years old with G1 functional pNETs in the body of pancreas. Perfusion map of the lesions in the body of pancreas at the same level was shown in (**A**-**Q**). (**R**-**T**) showed three-dimensional dual-source CT perfusion imaging in sagittal axis and coronal axis with the abdominal aorta used as the input artery (**U**). Region of interest was selected (**V**). The perfusion pseudo-color map of BF and BV was shown in (**W**-**X**). It could be seen that the lesion area was hyperperfused (arrow). Time density curves were shown in (**Y**), which showed that the enhancement pattern of the lesion was consistent with that of the adjacent normal pancreas, but the enhancement degree was higher than that of the normal pancreas

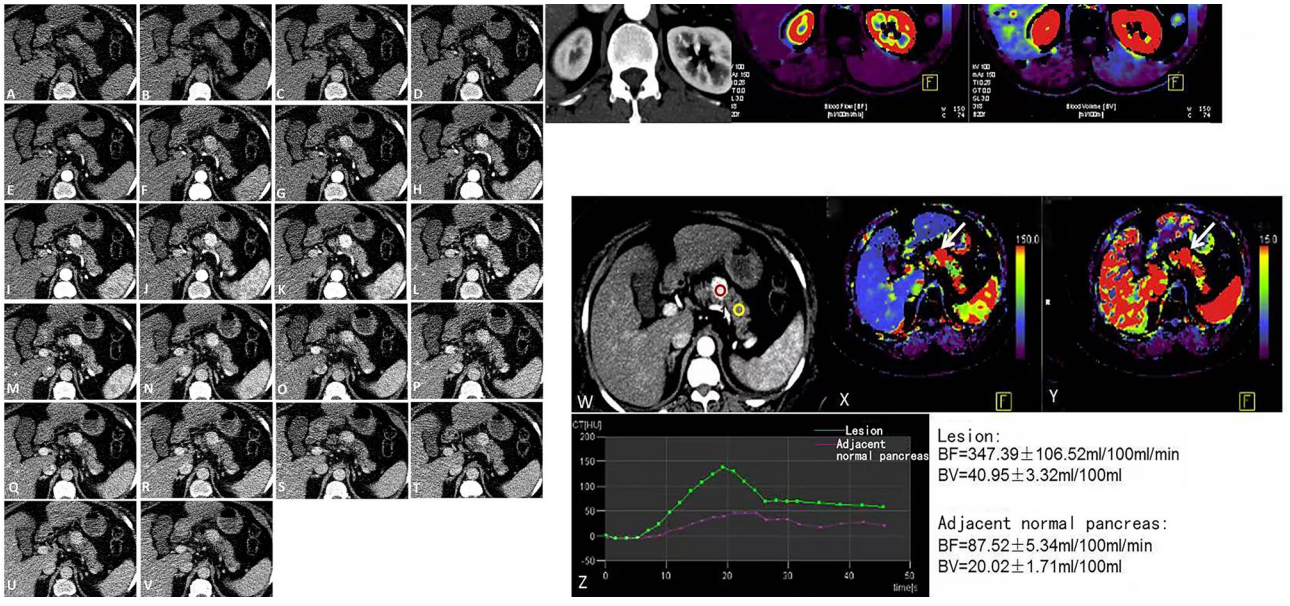

Fig. 5 Representative case with "fast-in and slow-out" enhancement of lesions. The female was 65 years old with G1 functional pNETs in the neck of pancreas. Perfusion map of the lesions in the body of pancreas at the same level was shown in (**A**-**V**). Region of interest was selected (**W**). The perfusion pseudo-color map of BF and BV was shown in (**X**, **Y**). It could be seen that the lesion area was hyperperfused (arrow). Time density curves were shown in (**Z**), which showed that the degree of enhancement of the lesion was significantly higher than that of the normal pancreas

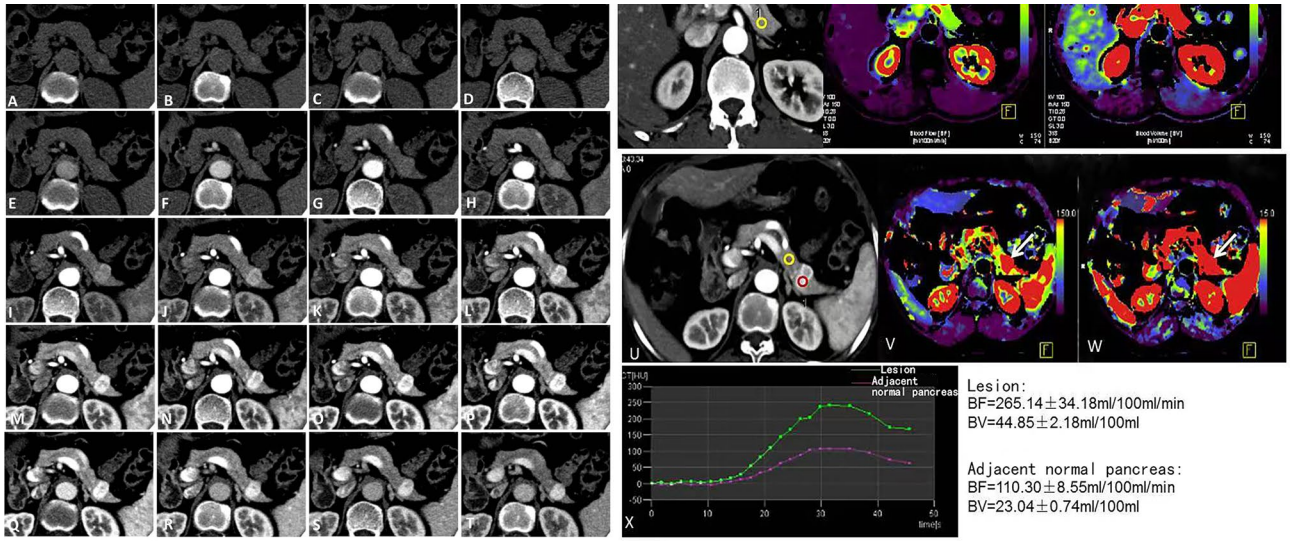

Fig. 6 Representative case with "slow-in and slow-out" enhancement of lesions. The female was 68 years old with G1 functional pNETs in the tail of pancreas. Perfusion map of the lesions in the body of pancreas at the same level was shown in (**A**-**T**). Region of interest was selected (**U**). The perfusion pseudo-color map of BF and BV was shown in (**V**, **W**). It could be seen that the lesion area was hyperperfused (arrow). Time density curves were shown in (**X**), which showed that the degree of enhancement of the lesion was significantly higher than that of the normal pancreas

Table 1 Statistical analysis of CT perfusion parameters of pNETs and adjacent normal pancreatic tissue ($n=26$, $\bar{x}\pm s$)

Perfusion parameters	*n*	Normal pancreatic tissue	pNETs	t	*P*
BF (mL/100mL/min)	26	144.32±55.35	336.61±216.72	4.470	<0.001
BV (mL/100mL)	26	28.64±7.95	41.96±16.99	4.147	<0.001
PS (mL/100 mL/min)	26	26.69±14.88	32.90±11.91	1.848	0.076
MTT (S)	26	12.89±3.69	9.44±4.40	4.655	<0.001
TTP (s)	26	20.33±5.18	19.14±5.6	3.846	0.001
TTS (S)	26	2.69±1.71	2.57±1.6	1.453	0.159

Table 2 Statistical analysis of CT perfusion parameters of well-differentiated pNETs and adjacent normal pancreatic tissue ($n=23$, $\bar{x}\pm s$)

Perfusion parameters	*n*	Normal pancreatic tissue	pNETs	t	*P*
BF (ml/100 ml/min)	23	140.52±49.73	370.72±206.55	5.434	<0.001
BV (ml/100 ml)	23	28.54±8.05	46.32±12.45	7.863	<0.001
PS (ml/100 ml/min)	23	24.18±7.89	33.96±11.91	3.927	0.001
MTT(S)	23	13.06±3.74	9.50±4.67	4.325	<0.001
TTP(s)	23	20.52±4.99	19.03±5.58	5.179	0.001
TTS(S)	23	2.82±1.77	2.67±1.65	1.606	0.123

supply in sSCA is related to the rich capillary components in tumor stroma, which are more abundant than pNETs [31]. In addition, pNETs should also be identified from tumors with rich blood supply around the pancreas, such as duodenal gastrointestinal stromal tumors (DST). For small pNETs tumors in the pancreatic head, they are usually functional tumors with related clinical symptoms. It is easy to distinguish from DST. However, for large pNETs lesions in the pancreatic head area, they are often non-functional and have no obvious clinical symptoms, similar to the enhancement characteristics of DST. It is usually necessary to carefully analyze the center of the lesion and the relationship between the lesion and the surrounding organs by multi-plane reconstruction images [32]. It should be noted that a small number of pNETs which lack blood supply need to be distinguished from pancreatic cancer and mass pancreatitis. Pancreatic cancer is a malignant tumor with the highest incidence of ischemia in the pancreas. It is characterized by an unclear margin, high invasiveness with metastasis of other organs and retroperitoneal lymph nodes, and often causes obvious dilation of pancreatic duct and bile duct, while the incidence of local invasion or metastasis of pNETs is low. Mass pancreatitis often has a clinical history of pancreatitis, be often accompanied by calcification along the pancreatic duct, and the boundary is unclear, showing

Table 3 Perfusion parameter values of normal pancreatic tissue and pNETs of different grades ($\bar{x}\pm s$)

Tissue	*n*	BF (mL/100 mL/min)	BV (mL/100 mL)	PS (mL/100 mL/min)	MTT (S)
Normal pancreatic tissue	26	144.32±55.35	28.64±7.95	26.69±14.88	12.89±3.69
Well- differentiated pNETs (G1/G2)	23	370.72±206.55	46.32±12.45	33.96±11.91	9.50±4.67
Poorly- differentiated pNETs (G3)	3	75.16±43.21	8.51±2.54	24.77±10.11	8.97±1.27

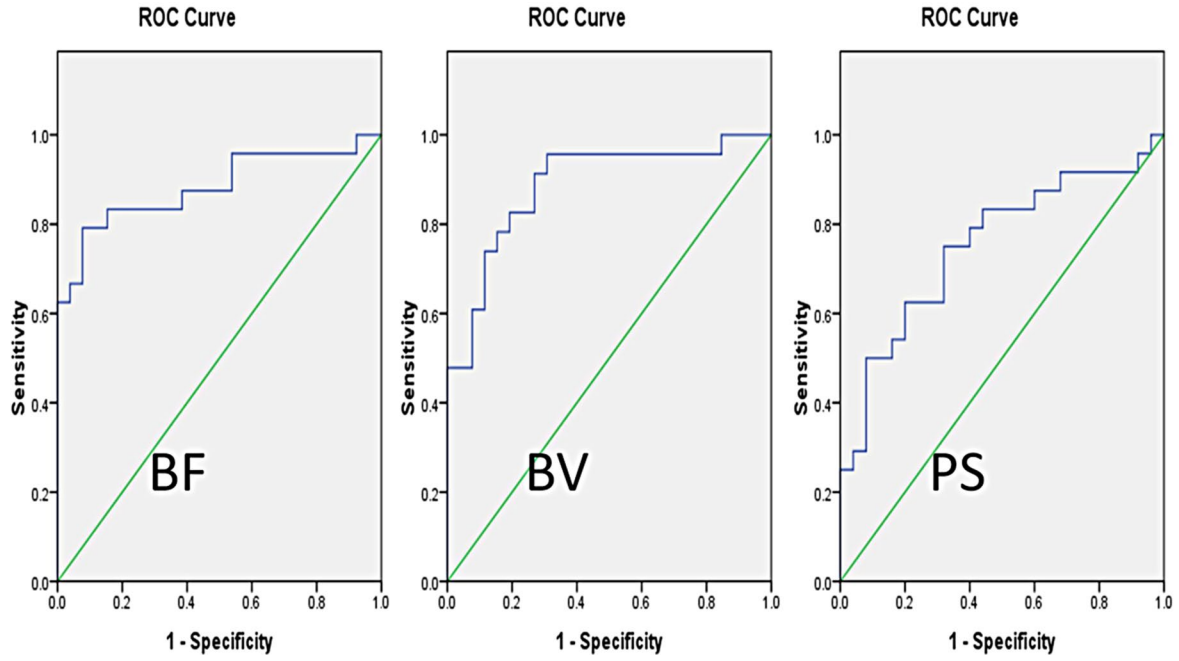

Fig. 7 ROC curves of the BF, BV, PS, with the area under the curve being 0.883, 0.886 and 0.752, respectively

Table 4 The diagnostic value of various perfusion parameters for pNETs

Perfusion parameters	Cutoff point	Sensitivity (%)	Specificity (%)	AUC of ROC
BF (mL/100 mL/min)	205.30	79.2	92.3	0.883
BV (mL/100 mL)	30.52	95.7	69.2	0.886
PS (mL/100 mL/min)	25.1	75	68	0.752

progressive enhancement. However, the CT values of pNETs lacking blood supply have little difference in each stage after enhancement [32–35].

In terms of pancreatic lesions, in addition to pNETs, CT perfusion imaging also has certain practicability in serous cystic tumors, mucinous cystic tumors, intraductal papillary mucinous tumors, suspected metastases, acinar cell carcinoma, acute and chronic pancreatitis [36]. However, due to its high radiation dose, CT perfusion imaging is limited in clinical application. It has been proposed that this technique can be combined with dual-energy computed tomography to reduce radiation exposure by at least 10%, in addition to the advantages of significantly reducing noise and metal artifacts, and reducing the dose of contrast agent [37]. In addition to providing useful value to tissues and tumors, CT perfusion has certain potential value in monitoring and evaluating patients' response to radiotherapy and chemotherapy, which needs to be further explored [38].

This study has several limitations. Firstly, the sample size was relatively small, and there was considerable variability among the included pNETs. The study showed that grade of pNETs was negatively correlated with perfusion parameters, which was inconsistent with results in previous study that only some perfusion parameters were in negative association with grade of pNETs. The reduced number of patients might lead to inconsistence, for which the conclusion in this study needs further study enrolling a large sample of patients to confirm. Patients with poorly differentiated pNETs (G3) was small, which limited credibility of results of comparisons in perfusion parameters between patients with well-differentiated pNETs and poorly-differentiated pNETs. However, the results demonstrated that Parameters like BF, BV, MTT, and TTP can effectively distinguish pNETs from adjacent healthy tissue. Patients with poorly differentiated pNETs were rarely enrolled for that the lesions are non-functional with no obvious symptoms. In order to improve the detection rate of pNETs, determination of enhanced scan time needs further study. Furthermore, the utility of CT perfusion imaging for characterizing tumor grades of pNETs lesions in a large sample of patients warrants further investigation.

Conclusions

In summary, CT perfusion imaging enables the dynamic visualization of contrast agent inflow and outflow, facilitating the accurate assessment of enhancement levels in pNETs lesions. Parameters like BF, BV, MTT, and TTP can effectively distinguish pNETs from adjacent healthy tissue. Moreover, the area under the ROC curve for BF, BV, and PS is clinically relevant in diagnosing pNET lesions.

Abbreviations

BF	Blood flow
BV	Blood volume
pNETs	pancreatic neuroendocrine tumors
PS	Permeability surface
ROC	Receiver Operating Characteristic
TDC	Time-Density Curve
TTP	Time to peak
TTS	Time to start

Acknowledgements
Not applicable.

Author contributions
Ge Liu collected and analyzed the data, obtained funds, and drafted the manuscript. Yan-Jun Gao collected the data, performed investigation, and obtained funds. Xiao-Bing Li conceptualized the study and edited the manuscript. Yi Huan conceptualized the study and analyzed the data. Jian Chen and Yan-Meng Deng analyzed the data and edited the manuscript. All authors read and approved the final draft.

Funding
This study was funded by the Key Research and Development Program of Shaanxi (Grant Number: S2018-YF-YBSF-0276). The funding body had no role in the design of the study and collection, analysis, and interpretation of data and in writing the manuscript.

Data availability
The datasets used and/or analyzed during the current study are available from the corresponding author upon reasonable request.

Declarations

Ethics approval and consent to participate
This study was conducted with approval from the Ethics Committee of Xi'an No. 3 Hospital (Approval Number: SYLL-2022-145). This study was conducted in accordance with the declaration of Helsinki. Written informed consent was obtained from all participants.

Consent for publication
Not applicable.

Competing interests
The authors declare no competing interests.

Received: 13 June 2024 / Accepted: 21 November 2024
Published online: 02 December 2024

References

1. Lawrence B, Gustafsson BI, Chan A, Svejda B, Kidd M, Modlin IM. The epidemiology of gastroenteropancreatic neuroendocrine tumors. Endocrinol Metab Clin North Am. 2011;40(1):1–18, vii. https://doi.org/10.1016/j.ecl.2010.12.005
2. Yao JC, Hassan M, Phan A, Dagohoy C, Leary C, Mares JE, Abdalla EK, Fleming JB, Vauthey JN, Rashid A, Evans DB. One hundred years after carcinoid: epidemiology of and prognostic factors for neuroendocrine tumors in 35,825 cases in the United States. J Clin Oncol. 2008;26(18):3063–72. https://doi.org/10.1200/JCO.2007.15.4377.
3. Scoazec JY, Couvelard A. Pour le réseau TENpath (réseau national d'expertise pour le diagnostic anatomopathologique des tumeurs neuroendocrines malignes de l'adulte, sporadiques et familiales). Une nouvelle classification OMS Des tumeurs (neuro)endocrines digestives [The new WHO classification of digestive neuroendocrine tumors]. Ann Pathol. 2011;31(2):88–92. https://doi.org/10.1016/j.annpat.2011.01.001. French.
4. Reid MD, Balci S, Saka B, Adsay NV. Neuroendocrine tumors of the pancreas: current concepts and controversies. Endocr Pathol. 2014;25(1):65–79. https://doi.org/10.1007/s12022-013-9295-2.
5. Jutric Z, Grendar J, Hoen HM, Cho SW, Cassera MA, Newell PH, Hammill CW, Hansen PD, Wolf RF. Regional Metastatic Behavior of nonfunctional pancreatic neuroendocrine tumors: impact of Lymph Node Positivity on Survival. Pancreas. 2017;46(7):898–903. https://doi.org/10.1097/MPA.0000000000000861.
6. Halfdanarson TR, Rubin J, Farnell MB, Grant CS, Petersen GM. Pancreatic endocrine neoplasms: epidemiology and prognosis of pancreatic endocrine tumors. Endocr Relat Cancer. 2008;15(2):409–27. https://doi.org/10.1677/ERC-07-0221.
7. Vignaux O, Gouya H, Augui J, Oudjit A, Coste J, Dousset B, Chaussade S, Legmann P. Hepatofugal portal flow in advanced liver cirrhosis with spontaneous portosystemic shunts: effects on parenchymal hepatic enhancement at dual-phase helical CT. Abdom Imaging. 2002 Sep-Oct;27(5):536 – 40. https://doi.org/10.1007/s00261-001-0095-7
8. Ichikawa T, Peterson MS, Federle MP, Baron RL, Haradome H, Kawamori Y, Nawano S, Araki T. Islet cell tumor of the pancreas: biphasic CT versus MR imaging in tumor detection. Radiology. 2000;216(1):163–71. https://doi.org/10.1148/radiology.216.1.r00jl26163.
9. Hiramoto JS, Feldstein VA, LaBerge JM, Norton JA. Intraoperative ultrasound and preoperative localization detects all occult insulinomas; discussion 1025-6. Arch Surg. 2001;136(9):1020–5. https://doi.org/10.1001/archsurg.136.9.1020
10. Machado MC, da Cunha JE, Jukemura J, Bacchella T, Penteado S, Abdo EE, Machado MA, Herman P, Montagnini AL, Pinotti H. Insulinoma: diagnostic strategies and surgical treatment. A 22-year experience. Hepatogastroenterology. 2001 May-Jun;48(39):854–8.
11. Khashab MA, Yong E, Lennon AM, Shin EJ, Amateau S, Hruban RH, Olino K, Giday S, Fishman EK, Wolfgang CL, Edil BH, Makary M, Canto MI. EUS is still superior to multidetector computerized tomography for detection of pancreatic neuroendocrine tumors. Gastrointest Endosc. 2011;73(4):691–6. https://doi.org/10.1016/j.gie.2010.08.030.
12. Lin XZ, Wu ZY, Tao R, Guo Y, Li JY, Zhang J, Chen KM. Dual energy spectral CT imaging of insulinoma-value in preoperative diagnosis compared with conventional multi-detector CT. Eur J Radiol. 2012;81(10):2487–94. https://doi.org/10.1016/j.ejrad.2011.10.028.
13. Zhu L, Xue HD, Sun H, Wang X, He YL, Jin ZY, Zhao YP. Isoattenuating insulinomas at biphasic contrast-enhanced CT: frequency, clinicopathologic features and perfusion characteristics. Eur Radiol. 2016;26(10):3697–705. https://doi.org/10.1007/s00330-016-4216-7.
14. Zhu L, Wu WM, Xue HD, Liu W, Wang X, Sun H, Li P, Zhao YP, Jin ZY. Sporadic insulinomas on volume perfusion CT: dynamic enhancement patterns and timing of optimal tumour-parenchyma contrast. Eur Radiol. 2017;27(8):3491–8. https://doi.org/10.1007/s00330-016-4709-4.
15. Yao JC, Phan AT, Hess K, Fogelman D, Jacobs C, Dagohoy C, Leary C, Xie K, Ng CS. Perfusion computed tomography as functional biomarker in randomized run-in study of bevacizumab and everolimus in well-differentiated neuroendocrine tumors. Pancreas. 2015;44(2):190–7. https://doi.org/10.1097/MPA.0000000000000255.
16. Miles KA, Hayball MP, Dixon AK. Measurement of human pancreatic perfusion using dynamic computed tomography with perfusion imaging. Br J Radiol. 1995;68(809):471–5. https://doi.org/10.1259/0007-1285-68-809-471.
17. Delrue L, Blanckaert P, Mertens D, Van Meerbeeck S, Ceelen W, Duyck P. Tissue perfusion in pathologies of the pancreas: assessment using 128-slice computed tomography. Abdom Imaging. 2012;37(4):595–601. https://doi.org/10.1007/s00261-011-9783-0.
18. Park MS, Klotz E, Kim MJ, Song SY, Park SW, Cha SW, Lim JS, Seong J, Chung JB, Kim KW. Perfusion CT: noninvasive surrogate marker for stratification of pancreatic cancer response to concurrent chemo- and radiation therapy. Radiology. 2009;250(1):110–7. https://doi.org/10.1148/radiol.2493080226.
19. Kambadakone AR, Sharma A, Catalano OA, Hahn PF, Sahani DV. Protocol modifications for CT perfusion (CTp) examinations of abdomen-pelvic tumors: impact on radiation dose and data processing time. Eur Radiol. 2011;21(6):1293–300. https://doi.org/10.1007/s00330-010-2048-4.
20. Bellomi M, Viotti S, Preda L, D'Andrea G, Bonello L, Petralia G. Perfusion CT in solid body-tumours. Part II: clinical applications and future development. Radiol Med. 2010;115(6):858–74. https://doi.org/10.1007/s11547-010-0545-9. English, Italian.
21. Kandel S, Kloeters C, Meyer H, Hein P, Hilbig A, Rogalla P. Whole-organ perfusion of the pancreas using dynamic volume CT in patients with primary pancreas carcinoma: acquisition technique, post-processing and initial results. Eur Radiol. 2009;19(11):2641–6. https://doi.org/10.1007/s00330-009-1453-z.
22. Diehl SJ, Lehmann KJ, Sadick M, Lachmann R, Georgi M. Pancreatic cancer: value of dual-phase helical CT in assessing resectability. Radiology. 1998;206(2):373–8. https://doi.org/10.1148/radiology.206.2.9457188.
23. Wan Y, Hao H, Meng S, Li Z, Yu F, chi, Meng et al. Application of low dose pancreas perfusion CT combined with enhancement scanning in diagnosis

of pancreatic neuroendocrine tumors. Pancreatology. 2021;21(1):240–245. https://doi.org/10.1016/j.pan.2020.10.046
24. Tsushima Y, Miyazaki M, Taketomi-Takahashi A, Endo K. Feasibility of measuring human pancreatic perfusion in vivo using imaging techniques. Pancreas. 2011;40(5):747–52. https://doi.org/10.1097/MPA.0b013e318215ac22.
25. Li HO, Sun C, Xu ZD, Miao F, Zhang DJ, Chen JH, Li X, Wang XM, Liu C, Zhao B. Low-dose whole organ CT perfusion of the pancreas: preliminary study. Abdom Imaging. 2014;39(1):40–7. https://doi.org/10.1007/s00261-013-0045-1.
26. Alexakis N, Neoptolemos JP. Pancreatic neuroendocrine tumours. Best Pract Res Clin Gastroenterol. 2008;22(1):183–205. https://doi.org/10.1016/j.bpg.2007.10.008.
27. Rindi G, Klöppel G, Alhman H, Caplin M, Couvelard A, de Herder WW, Eriksson B, Falchetti A, Falconi M, Komminoth P, Körner M, Lopes JM, McNicol AM, Nilsson O, Perren A, Scarpa A, Scoazec JY, Wiedenmann B. all other Frascati Consensus Conference participants; European Neuroendocrine Tumor Society (ENETS). TNM staging of foregut (neuro)endocrine tumors: a consensus proposal including a grading system. Virchows Arch. 2006;449(4):395–401. https://doi.org/10.1007/s00428-006-0250-1
28. D'Onofrio M, Gallotti A, Mantovani W, Crosara S, Manfrin E, Falconi M, Ventriglia A, Zamboni GA, Manfredi R, Pozzi Mucelli R. Perfusion CT can predict tumoral grading of pancreatic adenocarcinoma. Eur J Radiol. 2013;82(2):227–33. https://doi.org/10.1016/j.ejrad.2012.09.023.
29. d'Assignies G, Couvelard A, Bahrami S, Vullierme MP, Hammel P, Hentic O, Sauvanet A, Bedossa P, Ruszniewski P, Vilgrain V. Pancreatic endocrine tumors: tumor blood flow assessed with perfusion CT reflects angiogenesis and correlates with prognostic factors. Radiology. 2009;250(2):407–16. https://doi.org/10.1148/radiol.2501080291.
30. Ren S, Guo K, Li Y, Cao YY, Wang ZQ, Tian Y. Diagnostic accuracy of apparent diffusion coefficient to differentiate intrapancreatic accessory spleen from pancreatic neuroendocrine tumors. World J Gastrointest Oncol. 2023;15(6):1051–61. https://doi.org/10.4251/wjgo.v15.i6.1051.
31. Park HS, Kim SY, Hong SM, et al. Hypervascular solid-appearing serous cystic neoplasms of the pancreas: Differential diagnosis with neuroendocrine tumours. EUR RADIOL. 2015;26(5):1348–58. https://doi.org/10.1007/s00330-015-3961-3.
32. Ren S, Chen X, Wang J, Zhao R, Song L, Li H, Wang Z. Differentiation of duodenal gastrointestinal stromal tumors from hypervascular pancreatic neuroendocrine tumors in the pancreatic head using contrast-enhanced computed tomography. Abdom Radiol (NY). 2019;44(3):867–76. https://doi.org/10.1007/s00261-018-1803-x.
33. Ren S, Chen X, Wang Z, Zhao R, Wang J, Cui W, Wang Z. Differentiation of hypovascular pancreatic neuroendocrine tumors from pancreatic ductal adenocarcinoma using contrast-enhanced computed tomography. PLoS ONE. 2019;14(2):e0211566. https://doi.org/10.1371/journal.pone.0211566.
34. Guo CG, Ren S, Chen X, Wang QD, Xiao WB, Zhang JF, Duan SF, Wang ZQ. Pancreatic neuroendocrine tumor: prediction of the tumor grade using magnetic resonance imaging findings and texture analysis with 3-T magnetic resonance. Cancer Manag Res. 2019;11:1933–44. https://doi.org/10.2147/CMAR.S195376.
35. Ren S, Qian L, Daniels MJ, Duan S, Chen R, Wang Z. Evaluation of contrast-enhanced computed tomography for the differential diagnosis of hypovascular pancreatic neuroendocrine tumors from chronic mass-forming pancreatitis. Eur J Radiol. 2020;133:109360. https://doi.org/10.1016/j.ejrad.2020.109360.
36. Grözinger G, Grözinger A, Horger M. The role of volume perfusion CT in the diagnosis of pathologies of the pancreas. ROFO-FORTSCHR RONTG. 2014;186(12):1082–93. https://doi.org/10.1055/s-0034-1384876.
37. Wan Y, Hao H, Chen Y, et al. Application of spectral CT combined with perfusion scan in diagnosis of pancreatic neuroendocrine tumors. Insights Imaging. 2022;13(1):145. https://doi.org/10.1186/s13244-022-01282-9.
38. Sinitsyn V. Analysis and Interpretation of Perfusion CT in Oncology: type of Cancer matters. Radiology. 2019;292(3):636–7. https://doi.org/10.1148/radiol.2019191265.

Publisher's note